RSC Advances

This is an *Accepted Manuscript*, which has been through the Royal Society of Chemistry peer review process and has been accepted for publication.

Accepted Manuscripts are published online shortly after acceptance, before technical editing, formatting and proof reading. Using this free service, authors can make their results available to the community, in citable form, before we publish the edited article. This *Accepted Manuscript* will be replaced by the edited, formatted and paginated article as soon as this is available.

You can find more information about *Accepted Manuscripts* in the Information for Authors.

Please note that technical editing may introduce minor changes to the text and/or graphics, which may alter content. The journal's standard Terms & Conditions and the Ethical guidelines still apply. In no event shall the Royal Society of Chemistry be held responsible for any errors or omissions in this *Accepted Manuscript* or any consequences arising from the use of any information it contains.

ROYAL SOCIETY OF CHEMISTRY

www.rsc.org/advances

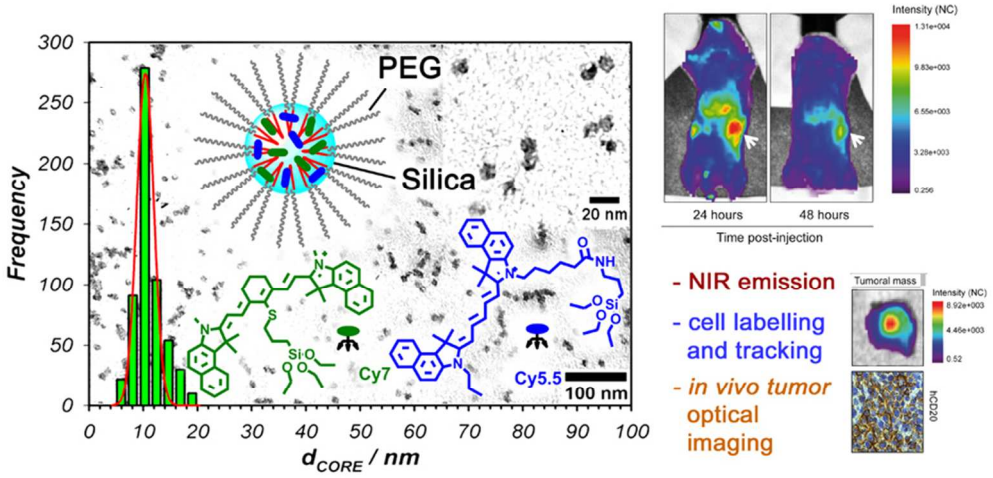

80x39mm (300 x 300 DPI)

RSC Advances Accepted Manuscript

RSCPublishing

ARTICLE

Multiple dye-doped NIR-emitting silica nanoparticles for both flow cytometry and *in vivo* imaging

Cite this: DOI: 10.1039/x0xx00000x

Stefania Biffi,[a] Luca Petrizza,[b] Enrico Rampazzo,[b] Rebecca Voltan,[c] Massimo Sgarzi,[b] Chiara Garrovo,[a] Luca Prodi,[b] Laura Andolfi,[d] Chiara Agnoletto,[c] Giorgio Zauli,[a] Paola Secchiero.[c]

Received ooth January 2014,
Accepted ooth January 2014

DOI: 10.1039/x0xx00000x

www.rsc.org/

Dye-doped near infrared-emitting silica nanoparticles (DD-NIRsiNPs) represent a valuable tool in bioimaging, because they provide sufficient brightness, resistance to photobleaching and consist of hydrophilic non-toxic materials. Here, we report the development of multiple dye-doped NIR emitting siNPs (mDD-NIRsiNPs), based on silica-PEG core-shell nanostructures doped with a donor-acceptor couple, exhibiting a tunable intensity profile across the NIR spectrum and suitable for both multiparametric flow cytometry analyses and time-domain optical imaging. In order to characterize the optical properties and fluorescence applications of the mDD-NIRsiNPs, we have characterized their performance by analyzing their *in vivo* biodistribution in healthy mice as well as in lymphoma bearing xenografts, and their suitability as contrast imaging agents for cell labeling and tracking. The mDD-NIRsiNPs features will be useful in designing new application for imaging agents based on silica nanoparticles for different experimental disease models.

Introduction

In the rapidly expanding field of biomedical imaging, there is a need for non-toxic, photostable and bright tools for fluorescent imaging. Optical imaging, based on fluorescence labeling, is in fact extensively applied to obtain functional information *in vivo* over time for the preclinical assessment of antibody binding, protein expression, enzymatic activities and cell tracking. For these reasons, it represents a rapidly improving technology for several applications.[1-6] In particular, optical imaging that exploits near-infrared (NIR) fluorescent light, has emerged as a tool also in the clinical context in order to provide real-time, intraoperative, high-contrast delineation of both normal and pathologic tissues and offers new prospects for general and oncologic surgery.[7] Indeed, fluorescence-guided surgery has the potential to improve cancer surgery outcomes, aiding surgeons in the identification and removal of malignant lesions. Therefore, over the last years much effort has gone in proof-of-concept clinical trials in this field.[8]

Despite the fact that several optical imaging approaches have been developed, there is an increasing need of more effective optical imaging probes beyond the approved indocyanine green (ICG).[7] In this context, significant advances have led to a variety of fluorescent labeling probes based on nanomaterials (nanoparticles; NPs), which allow to store large payloads of imaging contrast agents and/or therapeutics within the NP core and "tissue specific targeting" molecules on NP surface.[9] The versatility of synthetic NPs allows to provide contrast enhancement, binding specificity, improved stability and prolonged blood half-life.[10] Among the nanomaterials, fluorescent dye-doped NIR-emitting silica nanoparticles (DD-NIRsiNPs) have demonstrated excellent potential for applications in advanced bioanalysis.[9-12] DD-NIRsiNPs represent a valuable tool in bioimaging, since they provide sufficient brightness and photostability and consist of hydrophilic non-toxic materials.[13-15]

In this work, we have developed multiple dye-doped NIR emitting siNPs (mDD-NIRsiNPs) suitable for both time domain (TD) optical imaging and multiparametric flow cytometry analyses. In order to characterize the optical properties and fluorescence imaging applications of these mDD-NIRsiNPs, we have characterized their performance by analyzing their *in vivo* biodistribution in healthy mice as well as in lymphoma bearing xenografts, and their suitability as contrast imaging agents for cell labeling and tracking.

Results and Discussion

Synthesis and characterization of mDD-NIRsiNPs

RSC Advances Accepted Manuscript

RSCPublishing

ARTICLE

Table 1: Doping characteristics of the NPs samples presented in this study.

SiNPs sample	% *Dye* [a]	TEOS		Cy5.5[b]		Cy7[b]	
		µL	mmol	µmol	mg	µmol	mg
NP-1	0.1 ***Cy5.5***	180	0.8	0.8	0.65	-	-
NP-2	0.2 ***Cy5.5***	180	0.8	1.6	1.30	-	-
NP-3	0.2 ***Cy5.5*** – 0.1 ***Cy7***	180	0.8	1.6	1.30	0.8	0.71
NP-4	0.2 ***Cy5.5*** – 0.2 ***Cy7***	180	0.8	1.6	1.30	1.6	1.42

[a]doping ratio = [mol(**dye**)/mol(**TEOS**)]*100; [b]**Cy5.5** and **Cy7** were introduced in the reaction mixtures using pristine dichloromethane solutions.

The brightness of DD-NIRsiNPs depends both on the doping degree and on their photo-physical properties, since it is the result of a balance between the number of the dyes within the particle (that typically leads to an increase of the absorption coefficient) and their quantum yield. In the effort to design improved DD-NIRsiNPs we choose a core-shell silica-PEG structure to confer high colloidal stability properties, both *in vitro* and *in vivo*, with strongly reduced aggregation behaviour even in the presence of proteins.[10, 13] For optical imaging probes, as well as for cytometric applications, absorption emission properties suitable for our instrumentations was achieved doping our siNPs with the **Cy5.5** dye (Scheme 1 and Table 1: NP-1 and NP-2), whose polarity was suited for its insertion in the nanoparticle silica core.

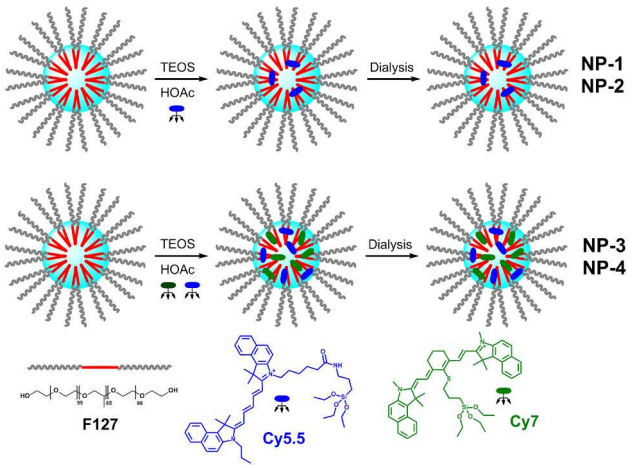

Scheme 1 Doping dyes (**Cy5.5** and **Cy7**) and schematization of the synthetic procedure used for the synthesis of the DD-NIRsiNPs (NP-1 and NP-2) and mDD-NIRsiNPs (NP-3 and NP-4) samples described in this work.

However, we found that this dye is considerably prone to aggregation, causing two main problems, both affecting total brightness: a loading inside the silica matrix lower than expected, and the occurrence of self-quenching processes,[14-16] which lead in this case to a large decrease of the fluorescence quantum yield of the **Cy5.5** dye inside the nanoparticles respect to the one observed in solution (see Table S1).

In particular, while the second effect has been already encountered and, with suitable strategies,[17, 18] minimized, the first one was quite unexpected. To circumvent these problems, we doped the DD-NIRsiNPs with two different cyanine dyes. The idea was to evaluate if the decrease in the probability of having aggregation among the same kind of dye could increase the siNPs doping and decrease the self-quenching phenomena. In addition, we also expected to have, at the same time, the beneficial effect of the presence of multiple signals.[9, 19] For this purpose, we synthesized mDD-NIRsiNPs containing the alkoxysilane derivative **Cy5.5** in combination with the IR813 alkoxysilane dye derivative **Cy7** (Scheme 1, Table 1: NP-3, NP-4 and ESI†). Different siNPs preparatives were synthesized by using increasing doping ratios of **Cy5.5**, used either alone (DD-NIRsiNPs; NP-1, NP-2) or in combination with **Cy7** (mDD-NIRsiNPs; NP-3, NP-4), at two different **Cy5.5**:**Cy7** molecular ratios (2:1, 1:1, Table 1). The synthesized siNPs present the typical absorption bands of **Cy5.5** (645 nm, 693 nm) and **Cy7** (828 nm). Additional morphological and photophysical properties of the siNPs are reported in ESI†.

As shown in Fig. 1, the four different siNP formulations were then assessed both by flow-cytometry as well as by optical imaging. In particular, for flow-cytometry assays, the formulations were used for cell-labeling, as previously reported.[20] Interestingly, mDD-NIRsiNPs doped with both fluorophores (NP-3 and NP-4) resulted in a signal detectable in the FL4 channel of the flow-cytometer, with a mean fluorescence intensity (NP-3 = 130; NP-4 = 100) significantly improved with respect to DD-NIRsiNPs doped with only **Cy5.5** (NP-1 = 16; NP-2 = 25) (Fig. 1A-B), showing that our approach was effective in increasing the siNPs brightness, because of a higher fluorescence quantum yield and a higher number of **Cy5.5** per nanoparticle. Similar results were obtained by comparing the fluorescence of the different mDD-NIRsiNPs samples with a small-animal TD fluorescence imager, with NP-3 exhibiting the best result with our experimental set up in terms of emission intensity, not only respect to NP-1 and NP-2 (**Cy5.5**, DD-NIRsiNPs) but also with respect to double dye NP-4 having comparable **Cy5.5** but the highest **Cy7** content (Fig. 1C). The NP-3 and NP-4 samples have in fact very similar overall quantum yields (Φ_{NP-3} = 0.08, Φ_{NP-4} = 0.06), but

RSC Advances Accepted Manuscript

different energy transfer efficiency (38% and 70%, respectively).

The NP-3 and NP-4 presented absorption and fluorescence emission properties related to their different donor-acceptor ratio, as shown in Fig. 1D. In particular, an increase in the **Cy5.5** fluorescence intensity was observed at lower **Cy7** concentration (NP-3). The presence of a higher **Cy7** concentration in NP-4 reduced the **Cy5.5** fluorescence intensity, due to the more efficient fluorescence energy transfer, as expected because of the increased concentration of the energy acceptor. As a result, NP-3 sample had an emission

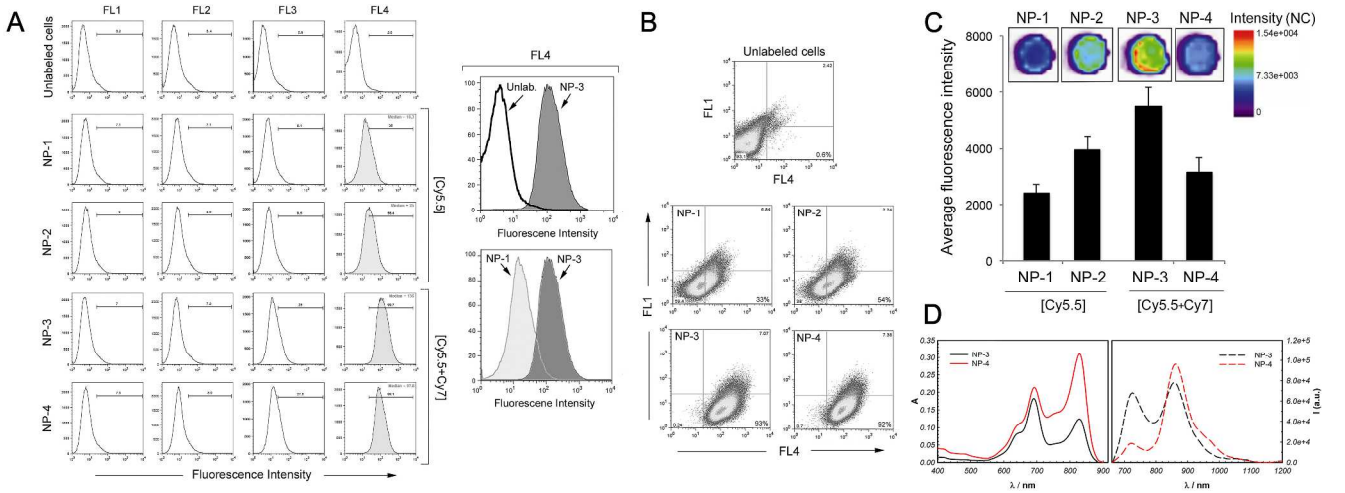

Fig. 1. Characterization of the flow-cytometric and optical imaging performance of the DD-NIRsiNPs and mDD-NIRsiNPs. (**A-B**) Cells were incubated with the indicated siNP preparatives at 37°C for 18 hours, to allow siNP cell internalization, before analyses by flow cytometry. (**A**) The fluorescence intensity of the DD-NIRsiNPs- and mDD-NIRsiNPs-labelled cells, detected selectively on the FL4 channel, is indicated by the light grey histograms. On the right panels, the overlays compare the fluorescence intensity of the double dye-doped NP-3 [**Cy5.5**+**Cy7**] either with the unlabeld cells (Unlab.) or with the single dye-doped NP-1 [**Cy5.5**]. (**B**) Flow-cytometric analyses of siNP-labeled cells are shown as dot plots; percentages of the positive cells (into the lower right quadrant) are indicated. (**C**) Equimolar aliquots of the siNP preparatives were placed on a paper substrate before analysis of the fluorescence with a time-domain fluorescence imager Optix. Results are expressed as means±SD of experiments performed in triplicate. (**D**) Comparison of absorption and emission spectra of the double dye-doped [**Cy5.5**+**Cy7**] samples NP-3 and NP-4. (**A-D**) For each set of analyses, representative results out of three independent experiments are shown.

profile matching more properly our experimental setup, with an improved brightness with respect to the other samples. For these reasons, we have chosen the sample NP-3 for the subsequent *in vivo* experiments carried out with our equipment. On the other hand, NP-4 could be conveniently used when optical imagers and/or cytometers have detectors in the 800 nm region.

Whole-body and *ex vivo* NIR fluorescence: analysis and biodistribution of mDD-NIRsiNPs

In the first set of experiments, NP-3 nanoparticles were deeply analyzed for their biodistribution. For this purpose, BALB/c mice were injected intravenously (i.v.) via the tail vein with 1 nmol of mDD-NIRsiNPs and analyzed by optical imaging. Whole-body fluorescence analysis revealed a diffuse distribution throughout the body of the mouse, at few minutes after i.v. injection of the mDD-NIRsiNPs and, within the first 24 hours, a strong signal was clearly detectable mainly in the liver and intestine decreasing over time (Fig. 2A). Of note, the mDD-NIRsiNPs associated fluorescent signal in the gastro-intestinal tract was highlighted by feeding the animal with special low-fluorescent chow. The fluorescence decay of mDD-NIRsiNPs was measured *in vitro* and a double exponential model was appropriately fitted (χ^2 = 1.03). This provided the possibility to discriminate *in vivo* between the tissues and the mDD-NIRsiNPs based both on fluorescence intensity and distinct lifetime profiles (data not shown).

To further investigate the extent of mDD-NIRsiNPs accumulation in the organs and tissues, mice were sacrificed at either 24 hours or 96 hours after i.v. injection of the mDD-NIRsiNPs, for *ex vivo* optical imaging analysis of explanted organs (i.e. kidneys, heart, spleen, brain, lungs, stomach, intestine, liver). This approach excludes any potential influence due to autofluorescence and scattering within the body and fur, thereby increasing both specificity and sensitivity of the probe detection. As shown in Fig. 2B-C, fluorescence intensity of the explanted organs was comparatively determined. At 24 hours after mDD-NIRsiNPs injection, the highest fluorescence signal was documented in the liver followed by intestine, kidneys, stomach, heart and lungs with the lowest signal observed in the spleen and in the brain (Fig. 2C). At 96 hours after mDD-NIRsiNPs injection, the isolated organs showed an overall decrease of the signal with respect to the 24 hours, with the highest fluorescence signal still in the liver and lowest signal in the heart and the brain (Fig. 2C), confirming the preferential localization of mDD-NIRsiNPs in the liver and a significant presence in the gastrointestinal tract. The localization of the mDD-NIRsiNPs within the organs was validated by fluorescence microscopic examination of tissue cryosections obtained from the explanted organs at 24 hours after mDD-

RSC Advances Accepted Manuscript

NIRsiNPs injection. Among the organs evaluated, maximum fluorescence signal was confirmed in the liver, which exhibited a homogeneously distributed NIR fluorescence along with NIR fluorescent spots, consistent with clusters of mDD-NIRsiNPs in the hepatic parenchyma (Fig. 2D). On the other hand, in contrast with the *ex vivo* analysis of the organs, negligible NIR fluorescence was observed in the small intestine wall sections (Fig. 2D). This apparent discrepancy was consistent with the presence of the mDD-NIRsiNPs in the feces (data not shown). Therefore, the overall observations derived by whole-body and *ex vivo* analyses are consistent with the excretion of the silica based nanostructures by the hepatobiliary way.[10] It is of interest

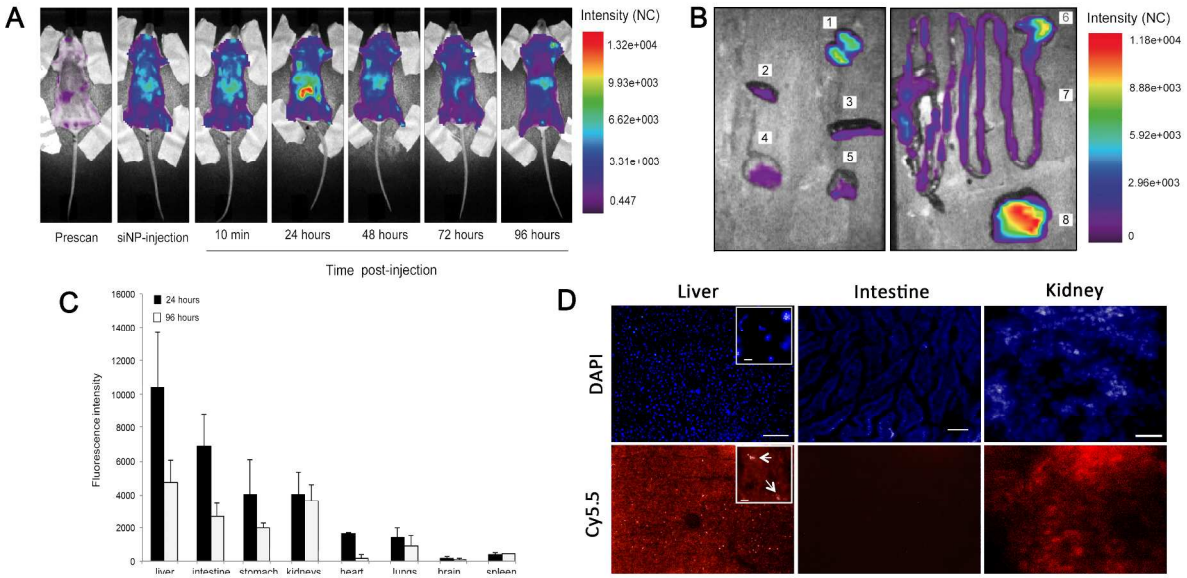

Fig. 2. Biodistribution of mDD-NIRsiNPs. BALB/c mice were injected intravenously (i.v.) via the tail vein with 1 nmol of mDD-NIRsiNPs and analyzed by optical imaging. (**A**) Whole-body scan of a representative mouse in supine position; fluorescence intensity images were acquired at the indicated time post-injection and are displayed in normalized counts (NC). (**B** and **C**) Mice were sacrificed at either 24 hours or 96 hours after i.v. injection of the mDD-NIRsiNPs, for *ex vivo* optical imaging analysis of the explanted organs. (**B**) *Ex vivo* imaging of organs explanted at 96 hours after mDD-NIRsiNPs administration are shown: 1, kidneys; 2, heart; 3, spleen; 4, brain; 5, lungs; 6, stomach; 7, intestine; 8, liver. (**C**) *Ex vivo* profile of mDD-NIRsiNPs distribution at 24 hours and 96 hours after i.v. injection. Data are expressed as means±SD of three independent experiments. (**D**) Representative fluorescence microscopy images of cryosections obtained from organs explanted from the mDD-NIRsiNPs injected mice. DAPI staining was carried out to visualize cell nuclei, which appear in blue, while mDD-NIRsiNPs appear in red; fluorescence images have identical exposure times to allow fluorescence comparison among tissues (liver, bar=150µm; intestine, bar=100µm; kidney, 50µm). The arrows into the inset indicate siNPs-clusters in the hepatic parenchyma (bar=5µm).

to note that, although microscopy of kidneys sections revealed a diffuse fluorescence signal (Fig. 2D), we did not detect any fluorescence in urine samples, indicating that the mDD-NIRsiNPs are above the threshold for renal clearance. These observations are in line with data previously reported showing that molecules with a hydrodynamic diameter > 8 nm do not typically undergo to glomerular filtration.[21]

mDD-NIRsiNPs as contrast agent for *in vivo* tumor imaging and cell tracking

Having characterized the biodistribution of mDD-NIRsiNPs in healthy mice, next experiments were carried out with the aim to evaluate the potential tumor-targeting properties of the mDD-NIRsiNPs.[22] For this purpose, the JVM-2 human leukemic cells were injected subcutaneously in SCID mice (10^7 cells/mouse), causing the formation of a tumor of an average size of 0.6-0.7 cm diameter in 12-15 days after injection.[23] At this point, subcutaneous tumor-bearing mice were i.v. injected with the mDD-NIRsiNPs and monitored for up to 48 hours (Fig. 3A). At 24 hours post-injection, *in vivo* whole-body TD optical imaging

RSC Advances Accepted Manuscript

This journal is © The Royal Society of Chemistry 2012

RSCPublishing

ARTICLE

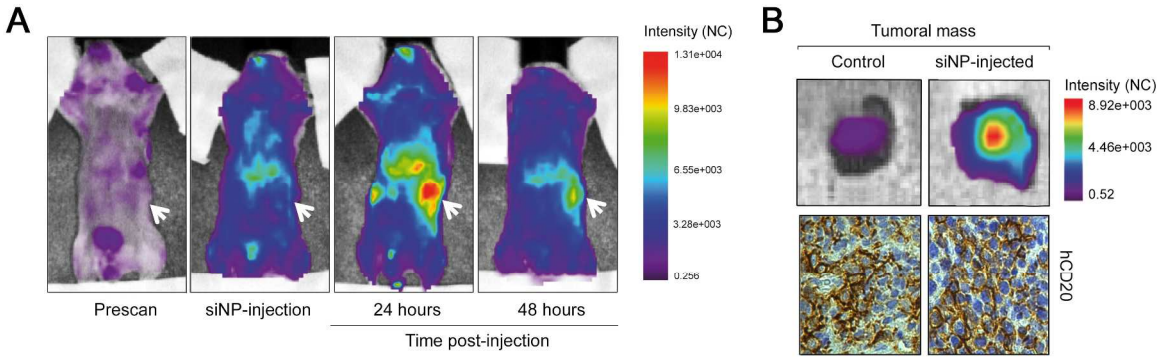

Fig. 3. Application of mDD-NIRsiNPs as contrast agent for *in vivo* tumor imaging. SCID mice (n=8) were subcutaneously injected with JVM-2 cells (10^7 cells/mouse) and, when xenograft tumors reached the size of 0.6-0.7 cm diameter, mice were either left untreated or i.v. injected with the mDD-NIRsiNPs. (**A**) Whole-body scan of a representative tumor-bearing mouse. Fluorescence intensity images were acquired at the indicated time post-injection; arrows indicate the tumor site. (**B**) *Ex vivo* imaging of the tumor mass explanted from mouse either left untreated or injected with mDD-NIRsiNPs. IHC analysis documents that the tumors derive from the s.c. injected $CD20^+$ JVM-2 cells (original magnification x200). Representative results are shown.

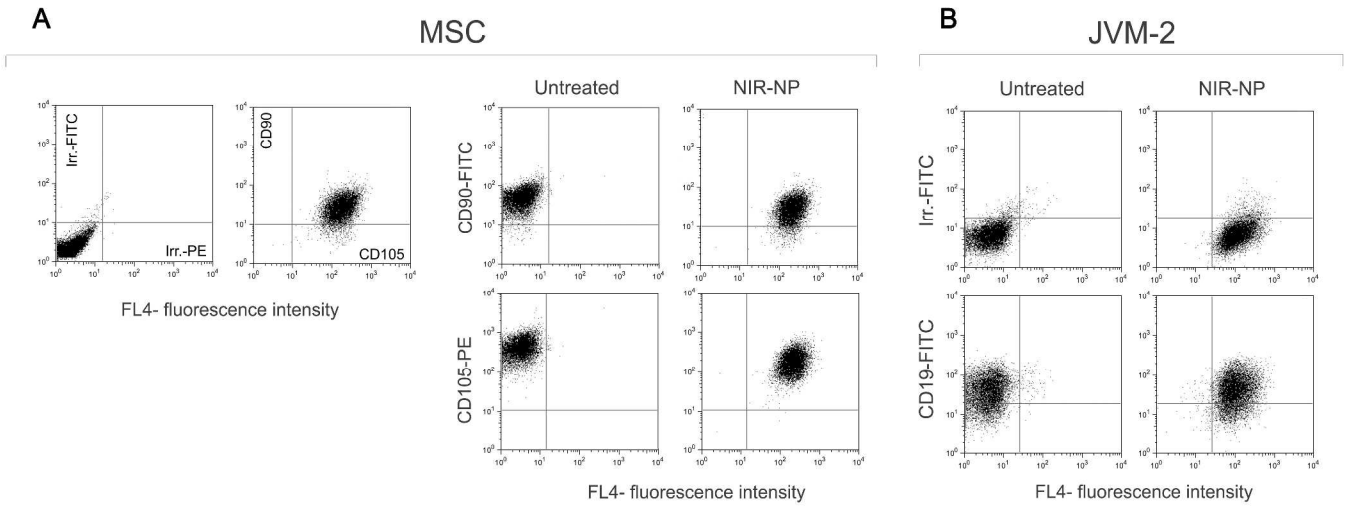

Fig. 4. mDD-NIRsiNPs allow multiparametric analysis in flow-cytometry. Cells were either left untreated or incubated with mDD-NIRsiNPs at 37°C for 18 hours, to allow siNPs cell internalization, before analyses by flow cytometry in combination with antibodies (Ab) for cell surface antigens. (**A**) MSC cells were labelled with mDD-NIRsiNPs along with both CD90 and CD105 Ab, using three different flow-cytometric channels. (**B**) JVM-2 cells were labelled with mDD-NIRsiNPs along with the B-cell specific CD19 Ab. Flow-cytometric analyses of multi-labeled cells are shown as two-colours dot plots in which co-expression (of either 2 different antigens or antigen+NP) is documented by localization of the cells in the upper right quadrant. Irr., isotype-matched control Ab. The results show that mDD-NIRsiNPs fluorescence does not interfere with the fluorescence (FITC, PE) of Ab used for phenotypical cell characterization. Representative results out of three independent experiments are shown.

clearly revealed a significant accumulation of mDD-NIRsiNPs in the tumor site, with a fluorescence that clearly delineated the subcutaneous tumor mass from the background of the surrounding tissues. The whole-body observations were confirmed by the *ex vivo* analysis of the explanted tumor masses, which allowed to confirm the localization of the mDD-NIRsiNPs-fluorescence signal into the JVM-2-derived tumor mass (Fig. 3B). At 48 hours after injection, although mDD-NIRsiNPs uptake was mainly in the liver, according to the hepatobiliary excretion, mDD-NIRsiNPs fluorescence was still

RSC Advances Accepted Manuscript

retained into the tumor mass to a significant extent. Our results clearly demonstrate the capacity of the circulating mDD-NIRsiNPs to passively localize into tumors due to the enhanced permeability and retention (EPR) effect, which is the result of leakiness of the tumor vasculature and impaired lymphatic drainage.[24] Of note, the tumor-targeting properties of mDD-NIRsiNPs could be suitable for important applications such as tumor imaging (for diagnostic purposes and for intraoperative image guidance) and/or to deliver drugs encapsulated in the mDD-NIRsiNPs core to the tumoral sites.

The lack of cell toxicity associated to these silica based-NPs,[10, 20] coupled to the fluorescence properties of the mDD-NIRsiNPs, allow their use for cell-labeling also in combination with specific surface cell antigens (conjugated to different fluorophores), as exemplified in Fig. 4A-B. To assess whether the mDD-NIR-siNPs can efficiently be used for applications combining flow-cytometry with optical imaging, we have next investigated the possibility to track *in vivo* cells labeled with the mDD-NIRsiNPs.[25] For this purpose, JVM-2 cells were labeled with mDD-NIRsiNPs and the efficiency of the intracellular uptake was verified by flow-cytometry (Fig. 4B), before s.c. injection in SCID mice. Injected mice were then monitored daily by whole-body TD optical imaging. As shown in Fig. 5A, a strong fluorescent signal was detectable in the injection site for 3 days after cell inoculation and, although the signal decreased progressively over time, it was still visible for 12 days. Of note, the signal was still associated to the mDD-NIRsiNPs-JVM-2 labeled cells, and not derived from cell-free nanoparticles, as confirmed by a couple of important evidences: 1) *ex vivo* and IHC analyses of the explanted subcutaneous tissue documented a co-localization of the fluorescence and of the human CD20 antigen (the marker of JVM-2 cells), respectively (Fig. 5B); 2) from day 8 onward a subcutaneous tumor mass became macroscopically detectable at the injection site (Fig. 5C), with a kinetics of growth in the next days comparable to that observed in mice injected with unlabeled JVM-2 (data not shown). Therefore, the tumor-forming capacity of mDD-NIRsiNPs-labeled cells provides a tool to monitor both the cell localization upon injection and the site of tumor development, anticipating/substituting eventual macroscopic manifestations or autoptic examinations in animal models.

Experimental

Nanoparticles synthesis

The preparation of core-shell silica-PEG (polyethylene glycol) dye doped nanoparticles was obtained adapting existing procedures (Scheme 1).[17, 18] For the preparation, 100 mg of Pluronic F127 and the desired amount of alkoxysilane dye(s)

RSC Advances Accepted Manuscript

This journal is © The Royal Society of Chemistry 2012

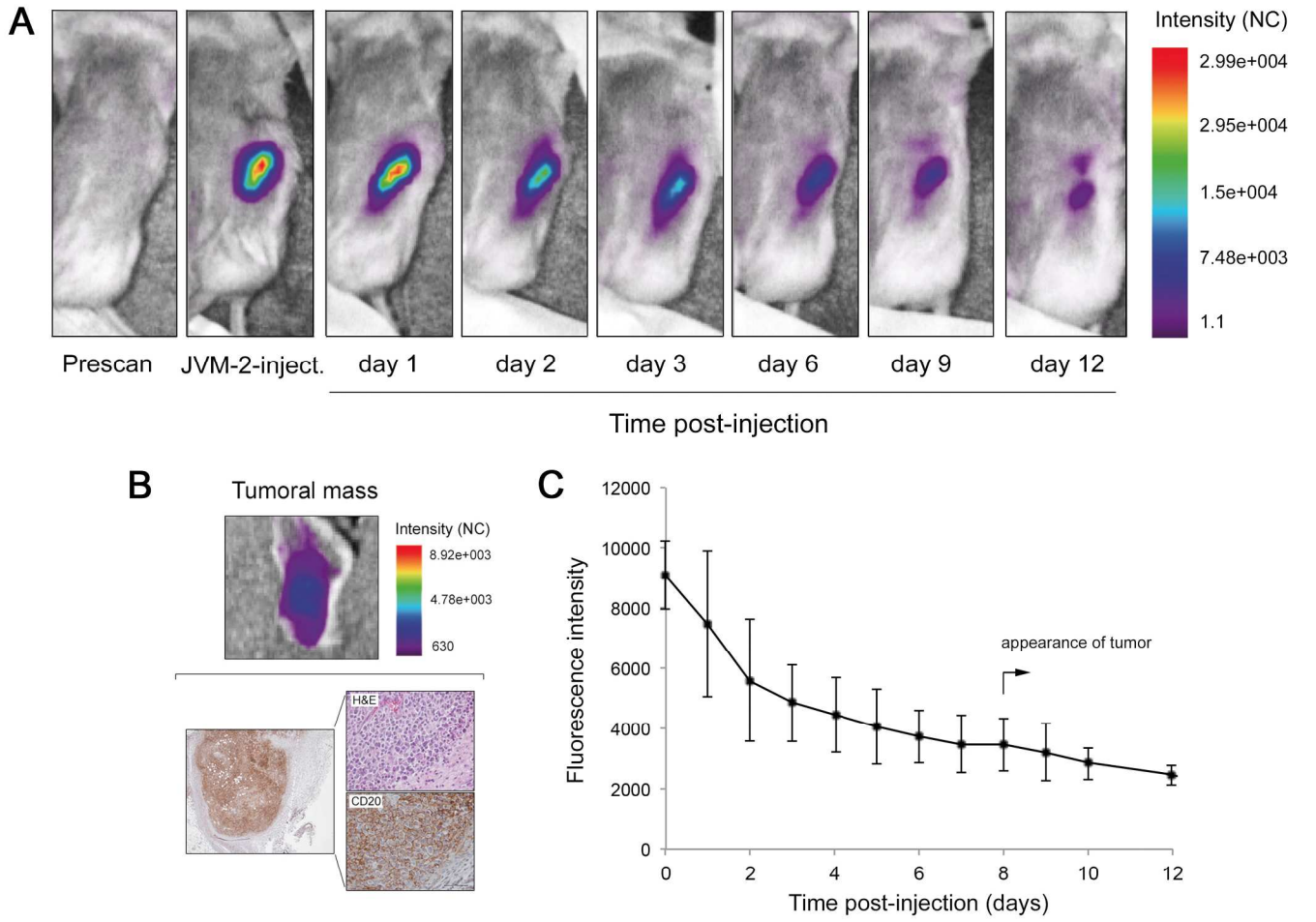

Fig. 5. *In vivo* cell tracking using mDD-NIRsiNPs as cell labeling probe. JVM-2 leukemic cells were either left untreated or incubated with mDD-NIRsiNPs at 37°C for 18 hours, to allow siNPs cell internalization, before s.c. injection in SCID mice (10^7 cells/mouse). (**A** and **B**) Whole-body scan of a representative mouse injected with mDD-NIRsiNPs-labeled JVM-2 and *ex vivo* imaging of the explanted subcutaneous tumor mass. Microscopic analyses of tumor sections stained with haematoxylin and eosin (H&E) and anti-human CD20 staining (original magnification x200) confirm the co-localization of the *in vivo* and *ex-vivo* fluorescence signal with the s.c. injected CD20+ JVM-2 cells. (**C**) At the indicated time post-injection of the labeled cells, fluorescence intensity images were acquired from whole-body scan of 5 mice and results are expressed as means±SD.

(Table 1) were solubilized with a small amount (~ 1.0 mL) of dichloromethane in a 20 mL glass scintillation vial. The solvent was then evaporated from the homogeneous solution under vacuum at room temperature.NaCl (68 mg) was added to the solid residue and the mixture was solubilized at 25°C under magnetic stirring with 1560 µL of acetic acid 1.0 M. TEOS (180 µL, 0.8 mmol) was then added to the resulting aqueous homogeneous solution followed by TMSCl (10 µL, 0.08 mmol) after 180 min. The mixture was kept under stirring for 48 hours at 25°C before dialysis treatments. The dialysis purification steps were carried out versus water on a precise amount of nanoparticles solution (1500 µL) finally diluted to a total volume of 5.0 mL with water.

Cells

JVM-2 B leukemic cell line was purchased from DSMZ (Deutsche Sammlung von Mikroorganismen und Zellkulturen GmbH, Braunschweig, Germany) and cultured in RPMI-1640 medium containing 15% FBS, L-glutamine, penicillin/streptomycin, supplemented with glucose 4.5 gL^{-1}, sodium pyruvate 1 mM, sodium bicarbonate 1.5 gL^{-1}, HEPES 10 mM (Gibco, Grand Island, NY).

Human bone marrow-derived mesenchymal stromal cells (MSC) were isolated as previously reported.[25] MSC cell preparations were homogenously CD105+, CD90+, CD34-, CD45-, CD14-, which is a typical MSC surface antigen profile, and were routinely cultured in MSC-Growth Medium (MSC-GM; Lonza, Walkersville, MD).

Flow cytometry analyses

Cell labeling performance and/or efficiency of the single and multiple DD-NIRsiNPs was quantitatively evaluated by flow cytometry using a FACSCalibur Analyzer (Becton-Dickinson, San Jose, CA) equipped with a 488 nm laser and a 635 nm laser, spatially separated. The filters used in our FACSCalibur provide the measurement of green (515-545 nm; FL1), yellow (564-606 nm; FL2), red (> 670 nm; FL3) fluorescences excited at 488 nm. The FL4 filter (653-669 nm) is used to measure the red fluorescence excited at 635 nm. This is possible because of

RSC Advances Accepted Manuscript

the particular hardware/elettronic setting, which allows the detection by the FL4 detector of the signals that have been exited by the 635 nm laser. For labeling of JVM-2, cells were seeded at 10^6 mL-1 in fresh medium before the addition of siNPs (10 nM). JVM-2 cultures were then placed at 37°C, 5% CO_2, for 18 hours. For cell labeling of adherent MSC cultures, siNPs were directly added to the medium of sub-confluent cell layer. Cultures were then kept at 37°C, 5% CO_2 for 18 hours. After 18 hours of incubation, cells were washed with PBS and incubated with 0.25% trypsin–EDTA (to remove any eventual residue of siNPs attached to the outside of cells and/or to detach MSC cells from the flask) and analyzed by flow cytometry. For multiparametric analysis, JVM-2 and MSC cultures, either left untreated or labeled with siNPs, were then incubated with the following monoclonal antibodies (Ab) recognizing cell-type specific surface antigens: FITC-conjugated anti-human-CD19 and PE-conjugated anti-human-CD105 (Immunotech; Marseille, France), FITC-conjugated anti-human-CD90 (Miltenyi Biotech, Auburn, CA). For cell surface staining, 5×105 cells were resuspended in 200 µL of PBS containing 1% BSA (Sigma-Aldrich, St Louis, MO) and incubated 30 minutes at 4°C with the conjugated monoclonal Ab (CD19 for the JVM-2 B cells; CD90 and CD105 for the MSC). Non-specific fluorescence was assessed by incubation of cells with isotype-matched conjugated Ab (Becton-Dickinson). Data files were collected and analysed using the CellQuest Pro software and displayed as single histograms and as two-colours dot plots to measure the proportion of double-positive cells.

Mice

Female BALB/c and SCID mice (4-6 weeks old) were purchased from Harlan (Italy) and maintained under pathogen-free conditions with ad libitum food and water, in accordance with the guide for the care and use of laboratory animals. All the experimental procedures were performed in compliance with the guidelines of European (86/609/EEC) and Italian (D.L.116/1992) laws and were approved by the institutional animal ethical care committee of the University of Trieste and by the Italian Ministry of Health. BALB/c mice were used for the biodistribution analysis of the mDD-NIRsiNPs in normal (healthy) settings, by i.v. injection of mDD-NIRsiNPs (1 nmol in 150 µL PBS, corresponded to 4.2 nmol of Cy5.5). SCID mice were used to establish xenograft tumor models by subcutaneous (s.c.) inoculation on the left flank of 10^7 human leukemic cells (JVM-2) resuspended in 100 µL of PBS. Explanted subcutaneous tumor masses, after *ex vivo* imaging acquisitions, were fixed in 10% buffered-formalin solution and embedded in paraffin for histological analysis.

Optical imaging assessment

Equimolar aliquots (20 µM) of the fluorescent single or multiple DD-NIRsiNPs preparatives were placed on a paper substrate and comparatively analyzed with a time-domain fluorescence imager Optix MX2 preclinical NIRF-imager (Advanced Research Technologies, Montreal, CA). The same equipment was adopted for the acquisition of *in vivo* data in mouse models, as previously described.[26] Briefly, mice were shaved prior to the scanning procedure in order to reduce scattering of the signal from fur. Throughout all imaging sessions, mice were anesthetized with vaporized isoflurane at 1.8-2.0 volume % (Sigma). The anesthetized mice were placed inside the acquisition system and gently fixed on a heated block (37°C) for the entire duration of data acquisition. Two-dimensional regions of interest (ROIs) were selected, and laser power, integration time (repetition time of the excitation per raster point) and scan step size were optimized according to the emitted signal. Prior to injection of the contrast agent (either mDD-NIRsiNPs or mDD-NIRsiNPs-labeled cells), mice were scanned to obtain background images. The background signal intensity, recorded with the baseline image for each animal, was subtracted from each post injection image. For *ex vivo* optical imaging, the last *in vivo* whole-body imaging session was followed by euthanasia of animals. The organs were explanted and imaged with the same Optix system. For each explanted organ, the average fluorescence intensity was calculated within a region of interest covering the whole sample and subtracted by the average fluorescence intensity within a region of the same area in the corresponding explanted organ of a control mouse (uninjected mouse). For selected mice, explanted organs were snap-frozen in isopentane and cooled at -80°C for tissue analysis.

Optical imaging results were analyzed by reporting fluorescence intensity values in normalized counts (NC) representing the photon count for unit excitation laser power and unit exposure time, allowing comparison among different images. Fluorescence lifetime results were obtained by fitting every fluorescence decay curve corresponding to each pixel measured by Optix using the Levenberg Marquet least squares method.[27]

Tissue analyses

For fluorescence microscopy, sections of 7- and 12-µm thickness were cut from frozen organs with a cryostat at -20°C. Glass slides were kept at 4°C at dark and Vectashield Mounting Medium with DAPI (Vector Laboratories, Burlingame, CA), diluted 1:1 with PBS, was used to stain cell nuclei. Fluorescent images were acquired by using an inverted microscope with a CCD camera (DVC-1412AM monochrome digital camera QE > 62% at 550nm) and the objectives lens 10x, 40x and 63x (NA 1.63) immersion oil.

For histological analysis, 5 µm thick sections were cut from paraffin blocks and stained with haematoxylin-eosin. Immunohistochemistry was performed by using the primary Ab for human CD20 (clone L26; NovocastraTM; Leica Biosystems Newcastle Ltd, Newcastle Upon Tyne, UK), associated to the NovoLinkTM Polymer Detection System (Novocastra), which was used for the visualization of the primary Ab, following manufacturer's instruction. After staining, the slides were examined under a Leica DM2000 optical microscope and microphotographs were taken using a Leica DFC320 digital camera.

RSC Advances Accepted Manuscript

 This journal is © The Royal Society of Chemistry 2012

Statistical analysis

Results from at least three independent experiments are reported as the means±SD and analyzed for statistical significance by the two-tail Student's t-test and Mann-Witney rank-sum test. Differences were considered significant when p value was < 0.05.

Conclusions

In this work, we have reported a synthetic strategy based on the development of silica-PEG core-shell nanostructures doped with a donor-acceptor couple exhibiting a tunable intensity profile across the NIR spectrum. This is a fundamental feature in view of applications such as whole-animal optical imaging and *in vitro* and *in vivo* cell labeling applications. In fact, this approach allows to increase the fluorescence signal *in vivo*, and to match in a versatile way the probe and experimental setup spectral properties. Moreover, it will be possible a significant improvement of the signal-to-noise ratio of optical measurements with respect to the single dye preparation, since large pseudo Stokes-shifts can be obtained exploiting efficient energy transfer processes within the particles.[17, 18, 24, 28, 29] These features will be useful in designing new application for imaging agents based on silica nanoparticles for different experimental disease models.

Acknowledgements

This work was supported by Consorzio SPINNER, and by grants from: MIUR (FIRB RBAP11Z4Z9_002 to G.Z.; FIRB RBAP10447J_002 to P.S.; PRIN 2009Z9ASCA and PON 01_01078 to LP) and Italian Association for Cancer Research (AIRC IG 11465 to G.Z.). The Authors are grateful to Andrea Lorenzon for his technical support for the experiments in mice models.

Notes and references

[a]Institute for Maternal and Child Health - IRCCS "Burlo Garofolo", via dell'Istria, 65/1, 34137 Trieste, Italy. Fax:+39-040-3785210; *Tel:+39-040-3785478*; E-mail: stefania.biffi@burlo.trieste.it.
[b]Department of Chemistry ''G. Ciamician'', University of Bologna, Via Selmi 2, 40126 Bologna, Italy. Fax:+39-051-2099456; Tel:+39-051-2099481; E-mail: luca.prodi@unibo.it.
[c]Department of Morphology, Surgery and Experimental Medicine and LTTA Centre, University of Ferrara, Via Fossato di Mortara 66, 44121 Ferrara, Italy. Fax:+39-0532-455950; Tel:+39-0532-455572; E-mail: paola.secchiero@unife.it.
[d]IOM-CNR TASC Laboratory, Basovizza, SS 14 km 163.5, 34149 Trieste, Italy. Fax:+39-040-226767; *Tel:+39-040-3756423*; E-mail: andolfi@iom.cnr.it.

† Electronic Supplementary Information (ESI) available: Fluorophore synthesis and characterization, TEM and DLS measurements, absorption and emission spectra and nanoparticles photophysical properties. See DOI: 10.1039/b000000x/

1. E. L. Kaijzel, G. van der Pluijm and C. W. Lowik, *Clin. Cancer Res.*, 2007, **13**, 3490.
2. J. O. McIntyre, R. L. Scherer and L. M. Matrisian, *Methods Mol. Biol.*, 2010, **622**, 279.
3. C. Agostinis, S. Biffi, C. Garrovo, P. Durigutto, A. Lorenzon, A. Bek, R. Bulla, C. Grossi, M. O. Borghi, P. Meroni and F. Tedesco, *Blood*, 2011, **118**, 4231.
4. K. E. Day, L. Sweeny, B. Kulbersh, K. R. Zinn and E. L. Rosenthal, *Mol. Imag. Biol.*, 2013, **15**, 722.
5. V. Ntziachristos and D. Razansky, *Recent Results Cancer Res.*, 2013, **187**, 133.
6. W. L. Byrne, A. DeLille, C. Kuo, J. S. de Jong, G. M. van Dam, K. P. Francis and M. Tangney, *J. Control. Release*, 2013, **172**, 523.
7. B. E. Schaafsma, J. S. Mieog, M. Hutteman, J. R. van der Vorst, P. J. Kuppen, C. W. Lowik, J. V. Frangioni, C. J. van de Velde and A. L. Vahrmeijer, *J. Surg. Oncol.*, 2011, **104**, 323.
8. A. L. Vahrmeijer, M. Hutteman, J. R. van der Vorst, C. J. van de Velde and J. V. Frangioni, *Nat. Rev. Clin. Onc.*, 2013, **10**, 507.
9. W. Bae, W. Tan and J.-I. Hong, *Chem. Commun.*, 2012, **48**, 2270.
10. M. Helle, E. Rampazzo, M. Monchanin, F. Marchal, F. Guillemin, S. Bonacchi, F. Salis, L. Prodi and L. Bezdetnaya, *ACS Nano*, 2013, **7**, 8645.
11. A. A. Burns, J. Vider, H. Ow, E. Herz, O. Penate-Medina, M. Baumgart, S. M. Larson, U. Wiesner and M. Bradbury, *Nano Lett.*, 2008, **9**, 442.
12. K. Ma, H. Sai and U. Wiesner, *J. Am. Chem. Soc.*, 2012, **134**, 13180.
13. M. Montalti, L. Prodi, E. Rampazzo and N. Zaccheroni, *Chem. Soc. Rev.*, 2014, DOI: 10.1039/c3cs60433k.
14. L. D. Lavis and R. T. Raines, *ACS Chem. Biol.*, 2008, **3**, 142.
15. H. J. Gruber, C. D. Hahn, G. Kada, C. K. Riener, G. S. Harms, W. Ahrer, T. G. Dax and H.-G. Knaus, *Bioconjugate Chem.*, 2000, **11**, 696.
16. S. Bonacchi, D. Genovese, R. Juris, M. Montalti, L. Prodi, E. Rampazzo and N. Zaccheroni, *Angew. Chem. Int. Ed.*, 2011, **50**, 4056.
17. E. Rampazzo, S. Bonacchi, R. Juris, M. Montalti, D. Genovese, N. Zaccheroni, L. Prodi, D. C. Rambaldi, A. Zattoni and P. Reschiglian, *J. Phys. Chem. B*, 2010, **114**, 14605.
18. D. Genovese, S. Bonacchi, R. Juris, M. Montalti, L. Prodi, E. Rampazzo and N. Zaccheroni, *Angew. Chem. Int. Ed.*, 2013, **52**, 5965.
19. J. L. Vivero-Escoto, R. C. Huxford-Phillips and W. Lin, *Chem. Soc. Rev.*, 2012, **41**, 2673.
20. E. Rampazzo, R. Voltan, L. Petrizza, N. Zaccheroni, L. Prodi, F. Casciano, G. Zauli and P. Secchiero, *Nanoscale*, 2013, **5**, 7897.
21. W. M. Deen, M. J. Lazzara and B. D. Myers, *Am. J. Physiol. Ren.*, 2001, **281**, F579.
22. A. Taylor, K. M. Wilson, P. Murray, D. G. Fernig and R. Levy, *Chem. Soc. Rev.*, 2012, **41**, 2707.
23. R. Voltan, P. Secchiero, B. Ruozi, F. Forni, C. Agostinis, L. Caruso, M. A. Vandelli and G. Zauli, *Clin. Cancer. Res.*, 2013, **19**, 3871.
24. H. Maeda, J. Wu, T. Sawa, Y. Matsumura and K. Hori, *J. Control. Release*, 2000, **65**, 271.
25. P. Secchiero, E. Melloni, F. Corallini, A. P. Beltrami, F. Alviano, D. Milani, F. D'Aurizio, M. G. di Iasio, D. Cesselli, G. P. Bagnara and G. Zauli, *Stem Cells*, 2008, **26**, 2955.
26. S. Biffi, S. Dal Monego, C. Dullin, C. Garrovo, B. Bosnjak, K. Licha, P. Welker, M. M. Epstein and F. Alves, *PLoS One*, 2013, **8**, e57150.
27. A. Abulrob, E. Brunette, J. Slinn, E. Baumann and D. Stanimirovic, *Mol. Imag. Biol.*, 2007, **6**, 304.

RSC Advances Accepted Manuscript

28. E. Rampazzo, S. Bonacchi, D. Genovese, R. Juris, M. Sgarzi, M. Montalti, L. Prodi, N. Zaccheroni, G. Tomaselli, S. Gentile, C. Satriano and E. Rizzarelli, *Chem. Eur. J.*, 2011, **17**, 13429.
29. D. Genovese, E. Rampazzo, S. Bonacchi, M. Montalti, N. zaccheroni and L. Prodi, *Nanoscale*, 2013, DOI: 10.1039/c3nr05599j.

RSC Advances Accepted Manuscript

 This journal is © The Royal Society of Chemistry 2012